



Supplement of

In-stream *Escherichia coli* modeling using high-temporal-resolution data with deep learning and process-based models

Ather Abbas et al.

Correspondence to: Kyung Hwa Cho (khcho@unist.ac.kr) and Laurie Boithias (laurie.boithias@get.omp.eu)

The copyright of individual parts of the supplement might differ from the article licence.

21

22

23

24 **Section S1. Study area and land use information**

25 The 0.6 km² Houay Pano catchment is part of the 800,000 km² Mekong River
26 basin. The catchment is located at an altitude of 435–716 m (Fig. 1) with a slope gradient
27 of 1 %–135 % (mean = 52 %). The closest village is Lak Sip, located downstream of station
28 S4 (Fig. 1), which has 484 inhabitants ([Census of 2015](#)).

29 The study area can be characterized as subhumid with a monsoon season. The dry season
30 stretches from November to May, whereas the wet season spans from June to October. The
31 annual mean temperature is 23.4 °C, and the annual mean precipitation is 1,366 mm from
32 2001 to 2019 ([Boithias et al., 2021](#)). However, during our study period (i.e., from 2011 to
33 2018), the mean annual precipitation was 1450 mm. Approximately 71 % of rainfall occurs
34 during the wet season. The subsurface geology predominantly consists of Permian to Upper
35 Carboniferous argillites, siltstones, and fine-grained sandstones. The soils in the study area
36 can be classified as Entisol, Ultisol, and Alfisol, comprising 20 %, 30 %, and 50 %,
37 respectively.

38 Detailed land-cover surveys and mapping were conducted each year from 2011 to
39 2018 within the catchment area. The annual areal percentages of fallow, teak trees, annual
40 crops, and forest were calculated using a geospatial information processing software QGIS
41 version 2.6 ([QGIS Development Team, 2016](#)) and denoted “Fallow,” “Teak,” “Annual
42 crop,” and “Forest,” for modeling purposes, respectively. The land-use change for each
43 type of land use is shown in the form of time series in Fig. S1. The area has recently

44 undergone an increase in teak tree plantations, especially from 2006 to 2013 (Ribolzi et al.,
45 2017). The fallow land use also increased at the expense of annual crops from 2012 to
46 2016.

47

48 **Section S2. Electrical-conductivity-based hydrograph separation**

49 We used a tracer-based approach (Collins and Neal, 1998) to separate storm
50 hydrographs into “event water” (infiltration-excess overland flow) and “pre-event water”
51 (groundwater pre-stored in the catchment area). This approach relies on a simple mixing
52 model with two reservoirs and the electrical conductivity of water as a tracer, and it had
53 been previously tested in the study catchment by Ribolzi et al., 2018). The tracer-based
54 approach is described by the following equations:

$$Q = Q_{OF} + Q_{GW}, \quad (1)$$

$$Q \times EC = Q_{OF} \times EC_{OF} + Q_{GW} \times EC_{GW}, \quad (2)$$

55 where Q is the instantaneous stream water discharge rate at the catchment outlet (m^3s^{-1});
56 Q_{OF} is the instantaneous discharge of overland flow—surface flow (m^3s^{-1}); Q_{GW} is the
57 instantaneous discharge of groundwater—subsurface flow (m^3s^{-1}); EC is the
58 instantaneous electrical conductivity measured in the stream ($\mu\text{S cm}^{-1}$); and EC_{OF} and
59 EC_{GW} are the electrical conductivity values in overland flow and groundwater ($\mu\text{S cm}^{-1}$).
60 EC_{OF} was measured in samples of overland flow collected at the soil surface on hillslopes
61 draining to the stream during the rainfall event (Ribolzi et al., 2018). Because groundwater
62 is supplied to the stream during interstorm flow periods, EC_{GW} was approximated from
63 stream measurements at the beginning of the flood event.

64

65 **Section S3. *E. coli* concentration monitoring and laboratory analysis**

66 The *E. coli* concentration was monitored at the gauging and sampling station by
67 collecting stream water samples (500 mL) in clean plastic bottles during both base flow
68 and stormflow events with an average frequency of 15 d. However, this sampling frequency
69 was not consistent over the 8 years, which led to a discontinuous time-series of *E. coli*
70 concentration. The water samples were kept in a cool box, and their analysis was carried
71 out within 24 h of collection.

72 To measure the *E. coli* concentration, we used the standardized microplate method
73 (ISO 9308–3). Each sample was incubated at four dilution rates (1:2, 1:20, 1:200, and
74 1:2000) in a 96-well microplate (MUG/EC, Biokar Diagnostics) for 48 h at 44 °C. Then,
75 the Ringers' Lactate solution was used for dilution, and one plate was used for each sample.
76 We then noted the number of positive wells for each microplate. The Poisson distribution
77 was used to calculate the most probable number (MPN) per 100 mL. This microplate
78 method has been successfully applied in other studies in the northern Lao PDR ([Ribolzi et](#)
79 [al., 2016](#); [Kim et al., 2017](#)).

80 Similar to grab sampling, we collected samples of stream water at the monitoring
81 station using clean plastic bottles and an automatic sampler (Automatic Pumping Type
82 Sediment Sampler, ICRISAT) for the measurement of *E. coli* concentration during 11 flood
83 events. The automatic sampler was triggered by the water level recorder to collect water
84 after every 2 cm of water-level change during the rising of the flood and after every 5 cm
85 of water level change during recession.

86

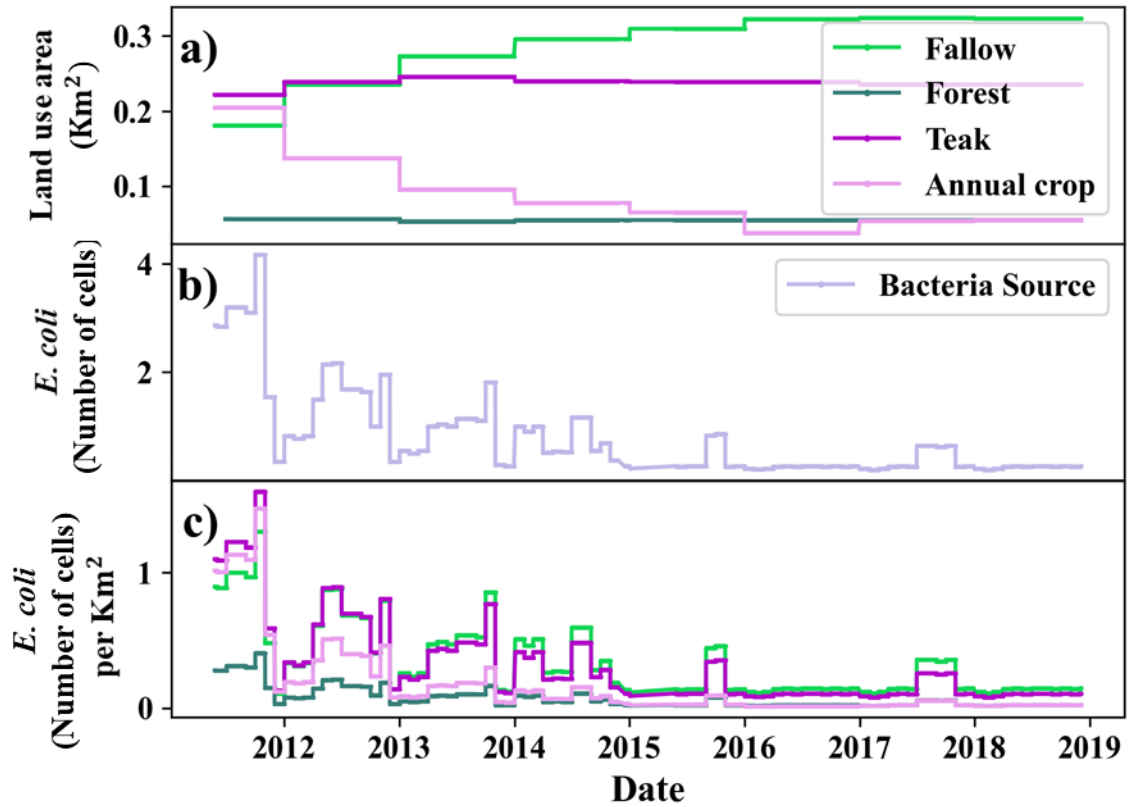
87 **Section S4. Sensitivity analysis and optimization**

88 During calibration processes, it is difficult to optimize a large number of parameters, so we
89 conducted a sensitivity analysis to determine which parameters affect the model output the
90 most. We used Python’s open-source library, “*SALib*” (Herman and Usher, 2017), to
91 implement the method of Morris, namely, one-at-a-time (OAT) (Morris, 1991). We used
92 13 PERLND-associated parameters (**Table S1**) for each land use for sensitivity analysis.
93 As our catchment included four land uses, the total number of parameters was 52. *SALib*
94 performed a sensitivity analysis by varying one variable at one time while keeping all other
95 variables constant. This process was repeated for all variables, and the model output was
96 recorded for each run. The model response in our case was the MSE value between the
97 simulated and predicted surface and subsurface flow. This method of Morris, which is
98 called the OAT method, has been used in many hydrological studies for sensitivity analysis
99 (van Griensvan et al., 2006; Baek et al., 2017; Cho et al., 2012). These parameters were
100 then ranked according to their sensitivity.

101 After sensitivity analysis, we calibrated the most sensitive parameters using the
102 truncated Newton algorithm (Nash, 1984) provided by the Scipy library (Jones et al., 2001)
103 of the Python programming language. During calibration, we optimized the model
104 parameters. The optimization we chose uses gradient information and optimized the
105 parameters between specific bounds. The bounds for all parameters are given in **Table S2**
106 and were taken from the literature (USEPA, 2000). The optimized values obtained after
107 calibration are given in **Table 3** in the manuscript.

108 We also conducted optimization based on different objective functions. We used
109 MSE and NSE calculated for simulated surface flow as well as for subsurface flow as an

110 objective function. During these optimization scenarios, the parameters of the HSPF, which
111 control the surface and subsurface flow, were optimized.
112



113

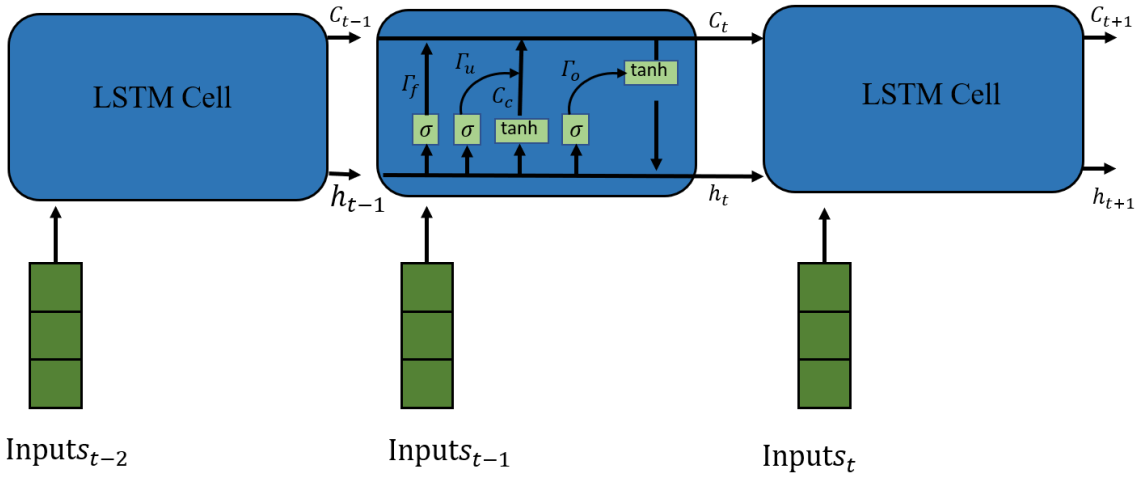
114 **Figure S1:** Land-use change and bacteria source from 2011 to 2018 in the Houay Pano

115 catchment, northern Lao PDR: (a) Land-use change, (b) Monthly variation of bacteria

116 source, and (c) *E. coli* source for each land use.

117

118



119

120 **Figure S2:** Description of an LSTM layer. An LSTM layer consists of LSTM cells which

121 process information at one time step and generates cell state (c_t) and hidden state (h_t)

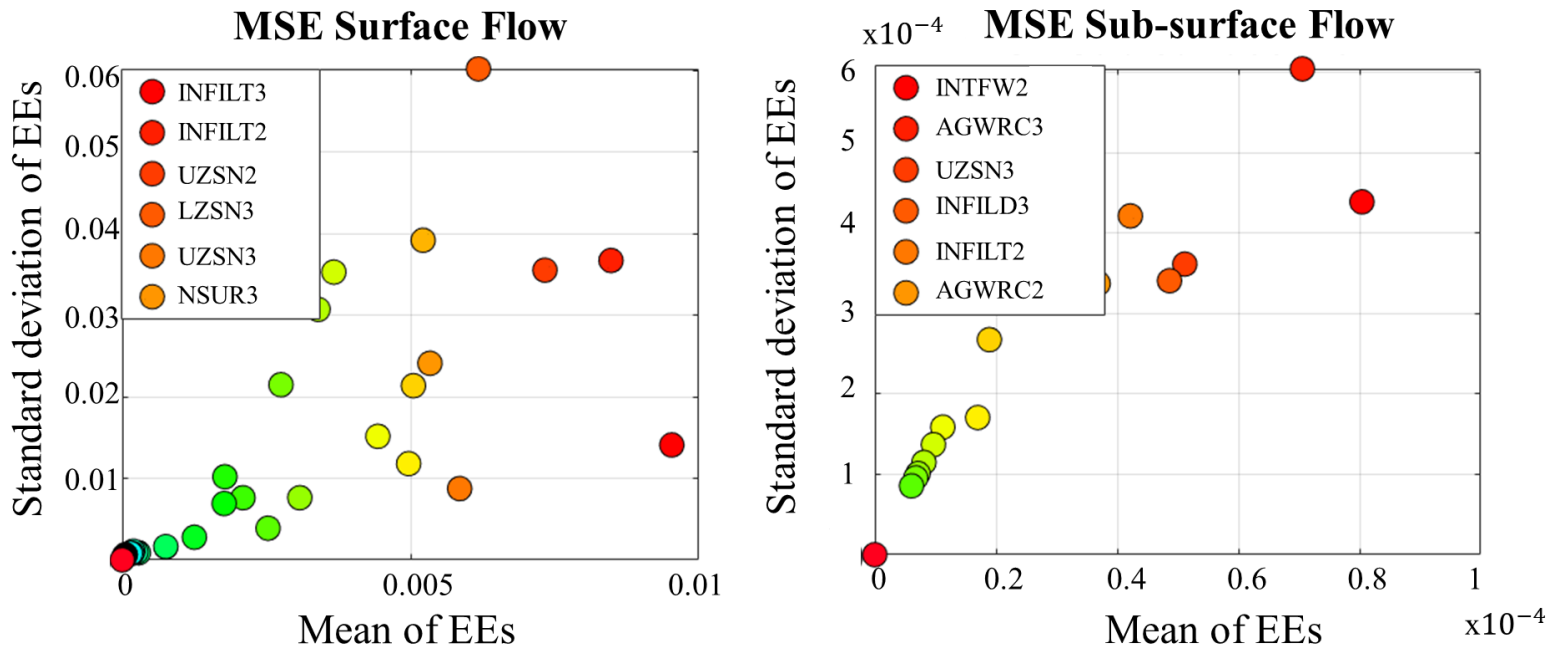
122 which are fed to the next LSTM cell. The hidden state is considered as output. The LSTM

123 cell consists of “forget” gate, “update” gate, and “output” gate. σ and \tanh represent

124 sigmoid and hyperbolic tangent nonlinearities

125

126



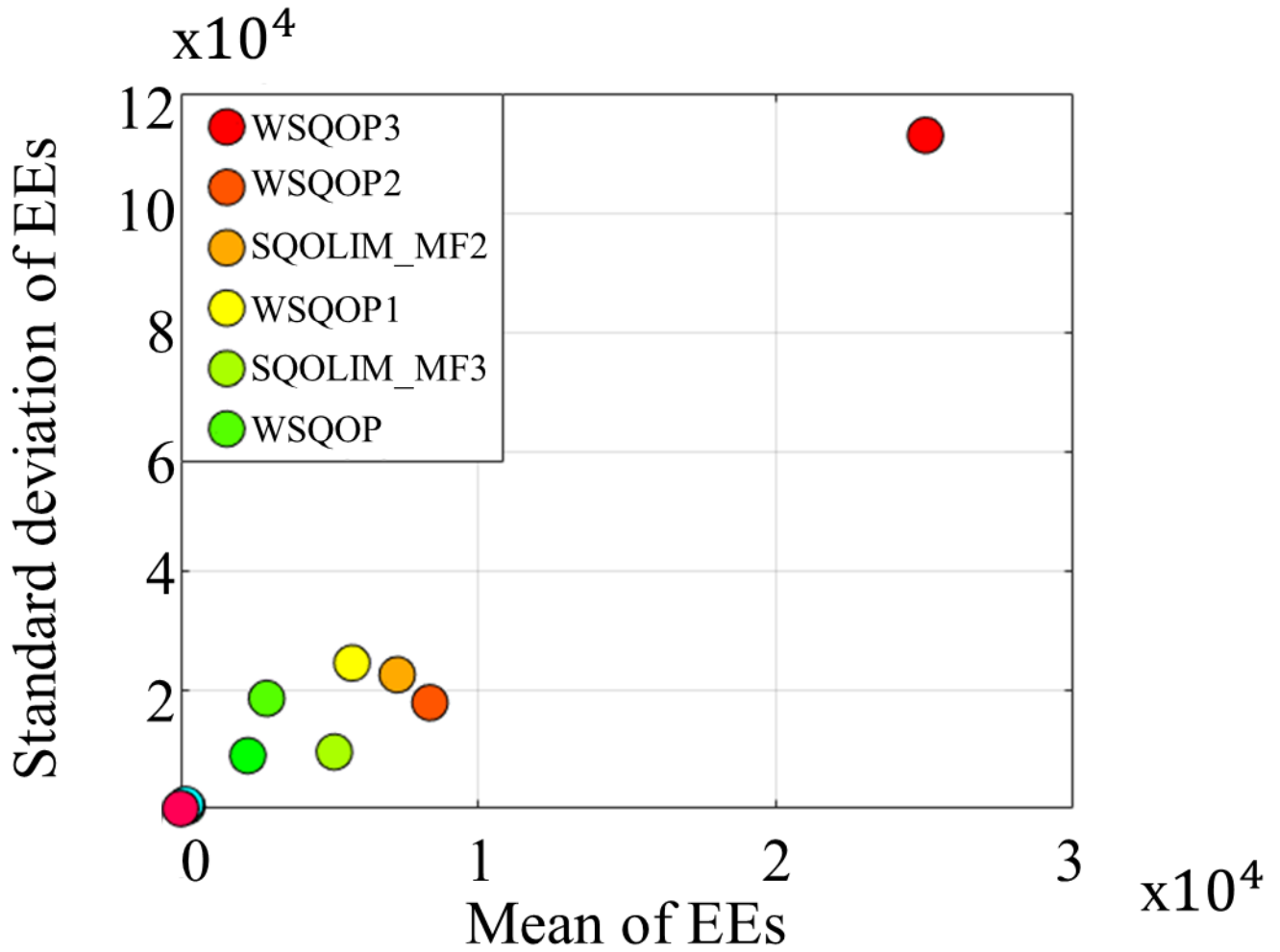
127

128 **Figure S3:** LH-OAT sensitivity analysis of hydrology parameters in HSPF. EEs

129 represent elementary effects. Details of abbreviations are given in Table S1. Boxes in

130 each plot show the five most sensitive parameters. Numbers in legends represent land

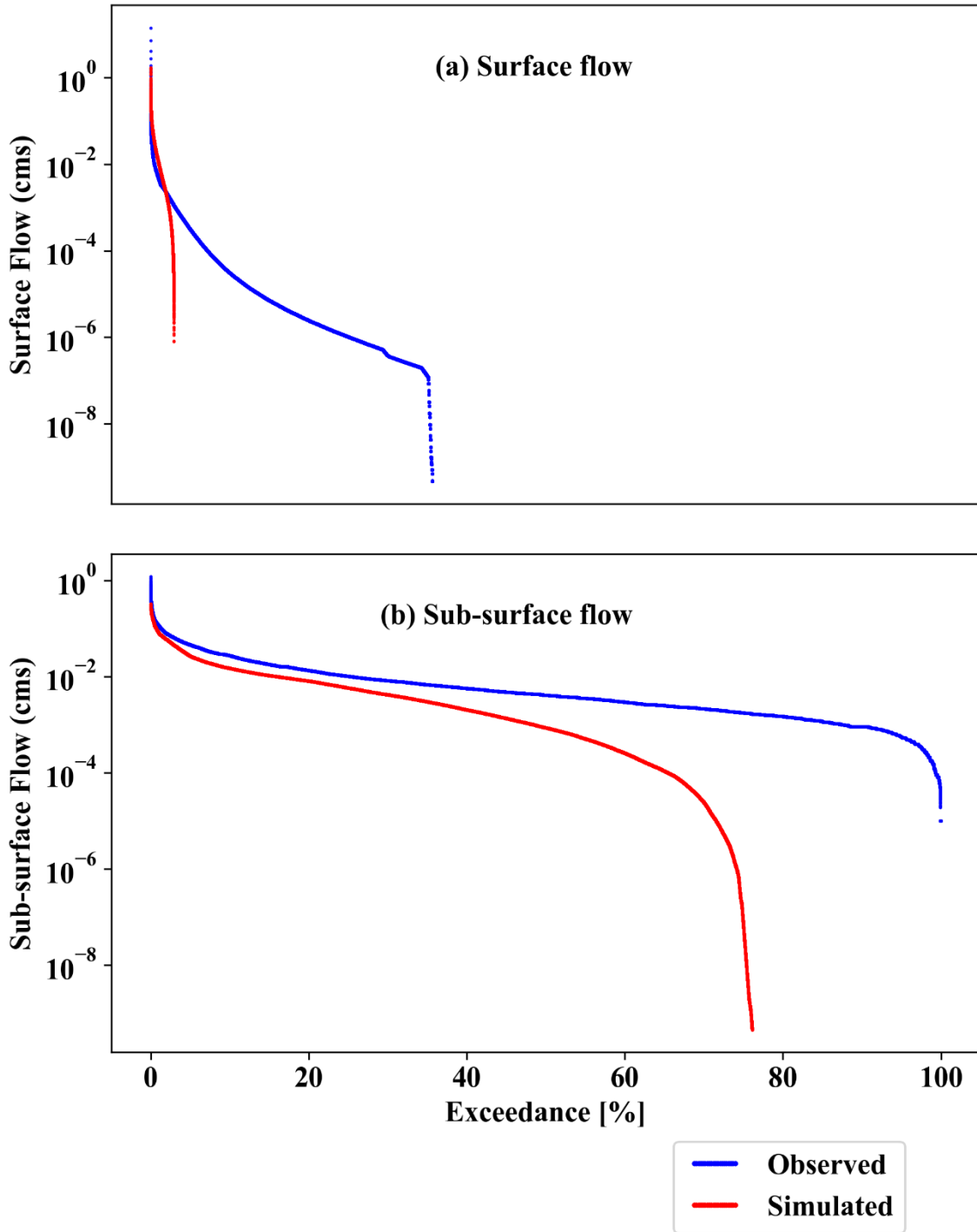
131 use; 1: Forest, 2: Teak, 3: Fallow, and 4: Annual crop.



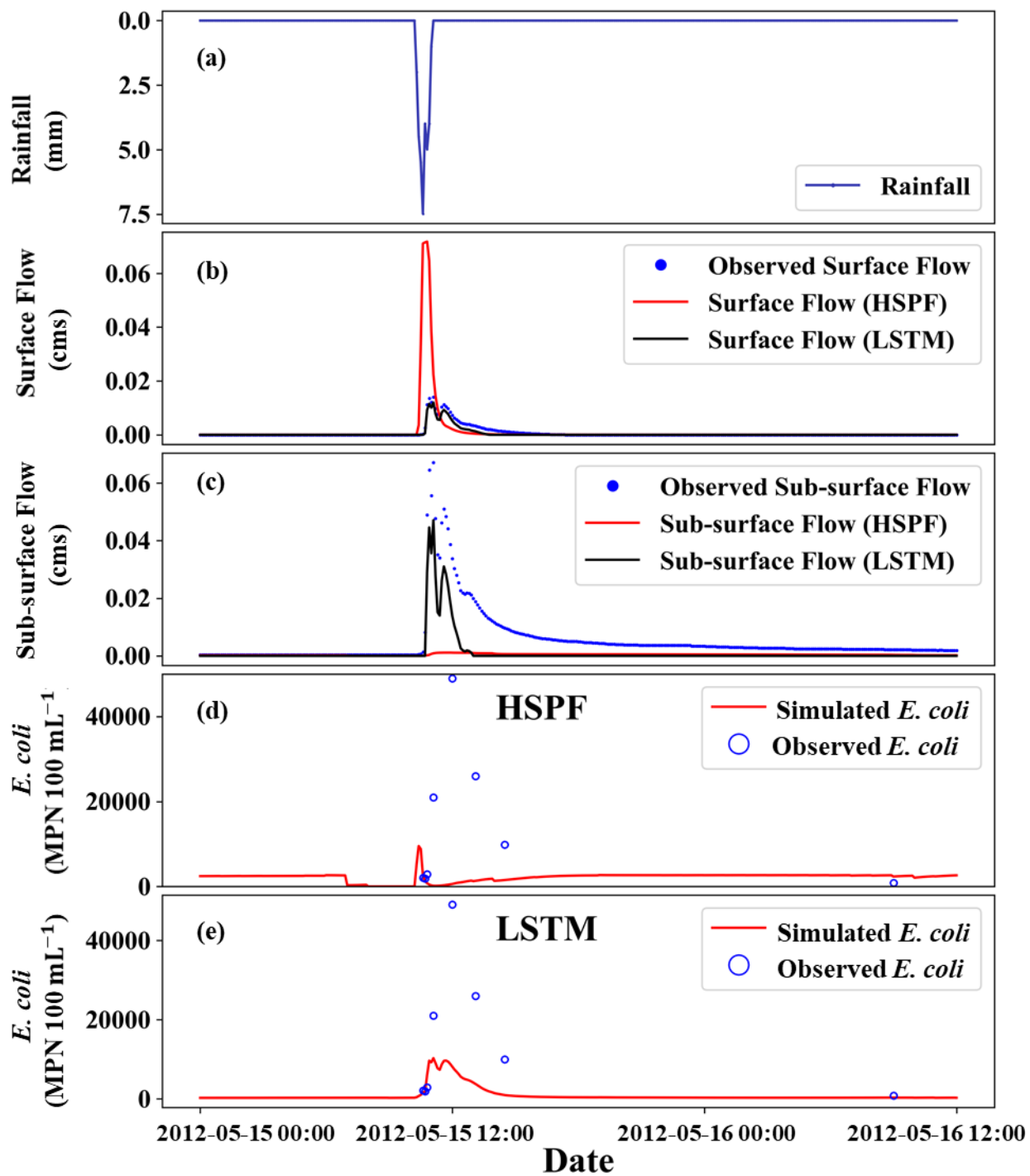
132

133

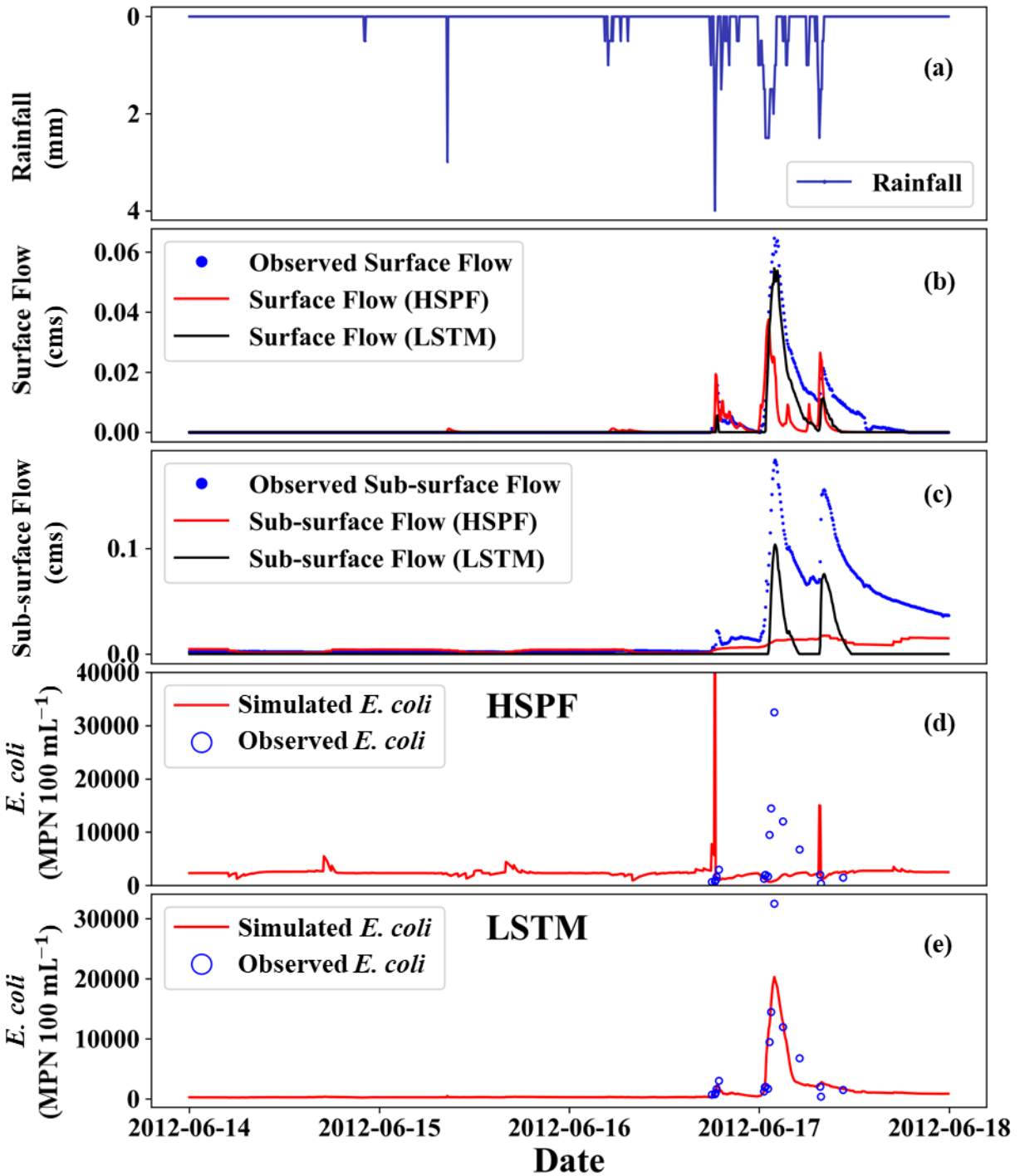
134 **Figure S4:** LH-OAT sensitivity analysis of *E. coli* parameters in HSPF. EEs represent
 135 elementary effects. Details of abbreviations are given in Table S1. Boxes in each plot
 136 show the five most sensitive parameters. Numbers in legends represent land use; 1:
 137 Forest, 2: Teak, 3: Fallow, and 4: Annual crop.



140 **Figure S5:** Flow duration curve for surface flow and subsurface flow from HSPF.



141
 142 **Figure S6:** *E. coli* concentration of HSPF and LSTM on May 15, 2012. (a) Observed rainfall, (b)
 143 Simulated and observed surface flow, (d) Simulated *E. coli* concentration from HSPF, and (d)
 144 Simulated *E. coli* concentration from LSTM.

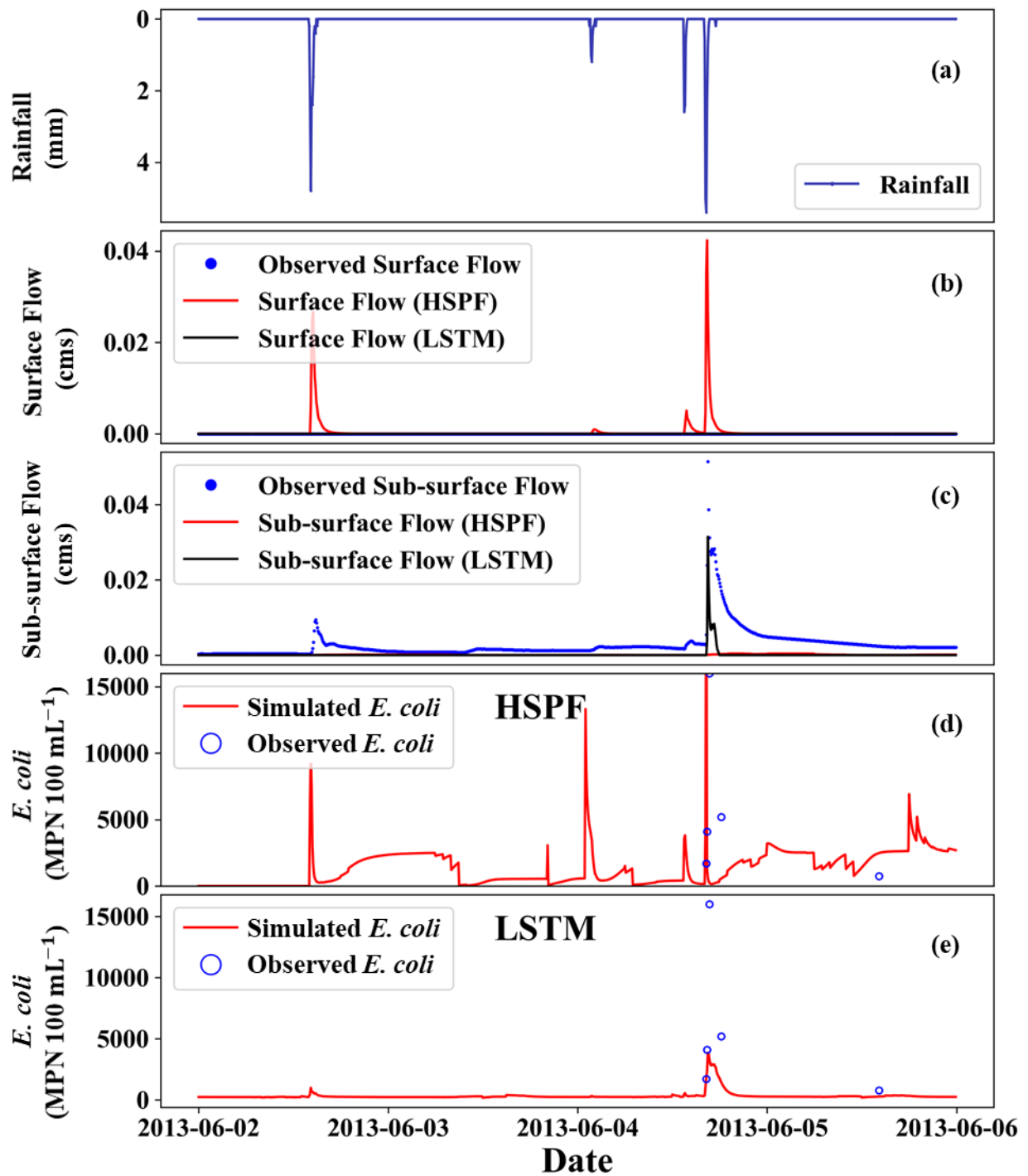


145

146 **Figure S7:** *E. coli* concentration of HSPF and LSTM on June 14, 2012. (a) Observed rainfall, (b)

147 Simulated surface flow, (c) Simulated subsurface flow, (d) Simulated *E. coli* concentration from

148 HSPF, and (d) Simulated *E. coli* concentration from LSTM.

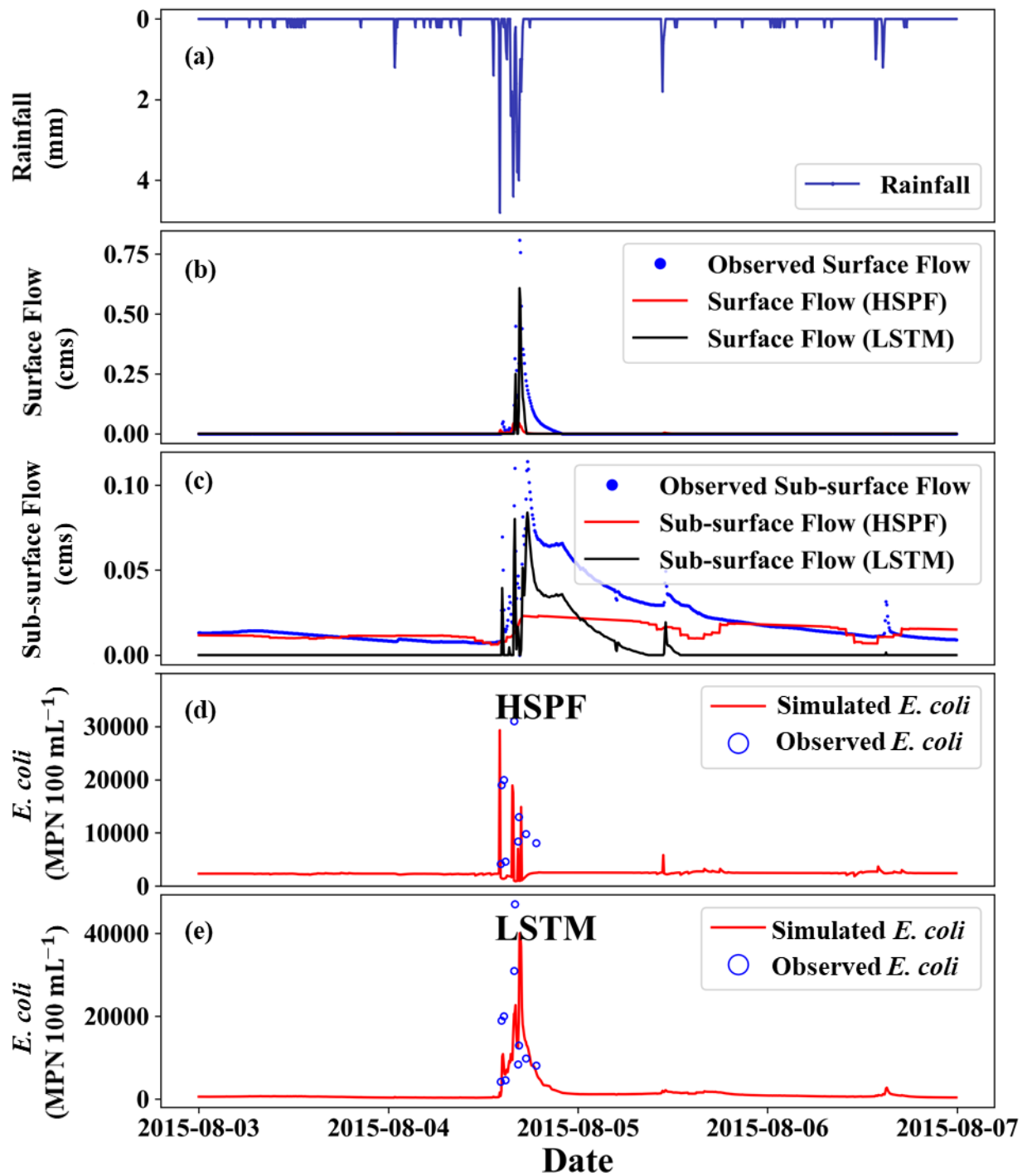


149

150 **Figure S8.** *E. coli* concentration of HSPF and LSTM on June 02, 2013. (a) Observed rainfall, (b)

151 Simulated surface flow, (c) Simulated subsurface flow, (d) Simulated *E. coli* concentration from

152 HSPF, and (d) Simulated *E. coli* concentration from LSTM.

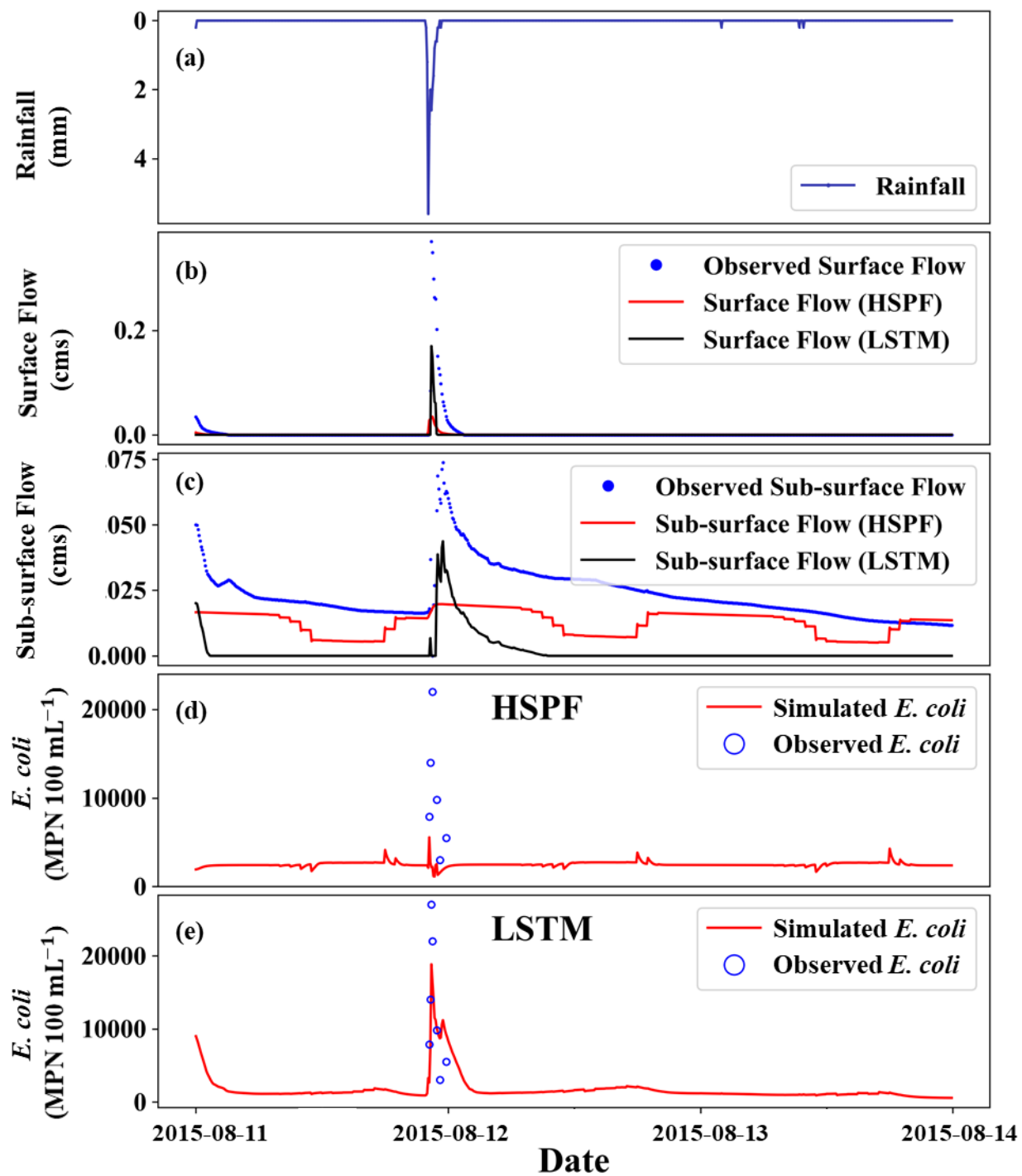


153

154 **Figure S9:** *E. coli* concentration of HSPF and LSTM on August 03, 2015. (a) Observed rainfall,

155 (b) Simulated surface flow, (c) Simulated subsurface flow, (d) Simulated *E. coli* concentration

156 from HSPF, and (e) Simulated *E. coli* concentration from LSTM.

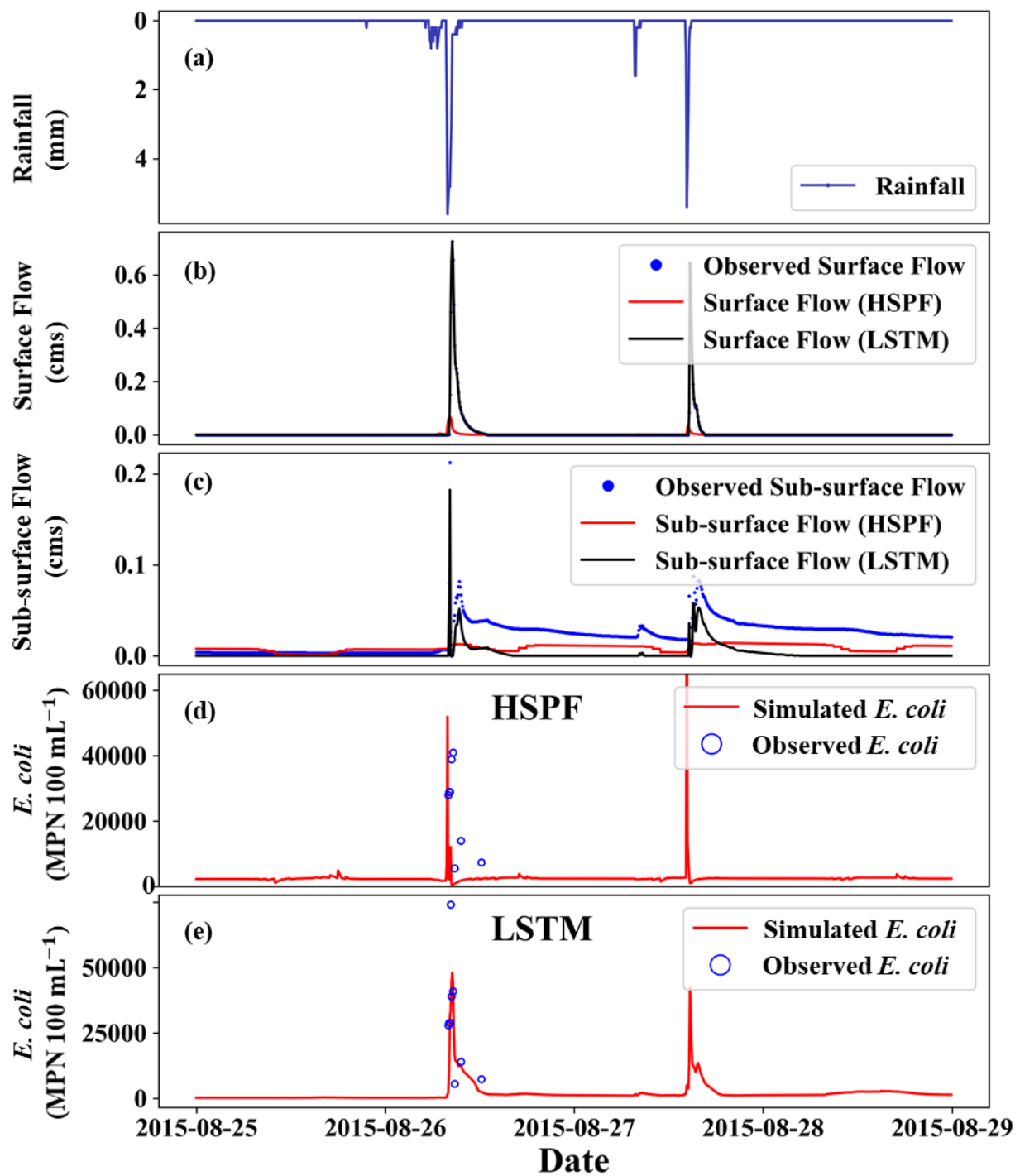


157

158 **Figure S10:** *E. coli* concentration of HSPF and LSTM on August 11, 2015. (a) Observed

159 rainfall, (b) Simulated surface flow, (c) Simulated subsurface flow, (d) Simulated *E. coli*

160 concentration from HSPF, and (d) Simulated *E. coli* concentration from LSTM.



161
 162 **Figure S11:** *E. coli* concentration of HSPF and LSTM on August 25, 2015. (a) Observed
 163 rainfall, (b) Simulated surface flow, (c) Simulated subsurface flow, (d) Simulated *E. coli*
 164 concentration from HSPF, and (e) Simulated *E. coli* concentration from LSTM.

165 **Table S1** Abbreviations of HSPF parameters

Abbreviation	Detailed Name
INFILT	Index to mean soil infiltration rate (inches/hour)
UZSN	Upper zone soil moisture storage (inches)
LZSN	Lower zone soil moisture storage (inches)
NSUR	Manning's n for overland flow plane
INFTEW	Interflow inflow parameter
INFILD	Ratio of max/mean infiltration capacities
BASETP	Fraction of remaining evapotranspiration from baseflow
DEEPR	Fraction of groundwater inflow to deep recharge
AGWETP	Fraction of remaining evapotranspiration from active groundwater
AGWRC	Base groundwater recession
FSTDEC	first-order decay rate for <i>E. coli</i>
THFST	Temperature Correction Coefficient for first-order decay of <i>E. coli</i>
SQOLIM	The maximum storage <i>E. coli</i> in the surface flow
WSQOP	the rate of surface flow that will remove 90 percent of stored <i>E. coli</i> in surface
	flow per hour.
ACQOP	the rate of accumulation of <i>E. coli</i> in surface flow.
AOQC	Concentration of <i>E. coli</i> in active groundwater flow
IOQC	Concentration of <i>E. coli</i> in Interflow

166

167

168

169 **Table S2** Sensitivity ranking of HSPF parameters for surface and subsurface flow with respect to
 170 Mean Square Error. Numbers represent land-use; 1: Forest, 2: Teak, 3: Fallow, and 4: Annual
 171 crop

Rank	Surface Flow	Subsurface flow
1	INFILT3	INTFW2
2	INFILT2	AGWRC3
3	UZSN2	UZSN3
4	LZSN3	INFILD3
5	UZSN3	INFILT2
6	NSUR3	AGWRC2
7	LZSN2	UZSN2
8	INFILT4	INFILT3
9	INTFW3	INTFW3
10	INTFW2	INFILT4
11	LZSN4	NSUR3
12	INFILD4	UZSN4
13	NSUR2	INFILD2
14	NSUR4	INTFW1

15	UZSN4	DEEPFR2 172
16	INFILD3	LZSN1
17	INFILD2	LZSN2
18	INTFW4	LZSN3
19	INFILT1	LZSN4
20	INTFW1	INFILT1
21	UZSN1	AGWRC1
22	NSUR1	AGWRC4
23	LZSN1	INFILD4
24	BASETP3	DEEPFR1
25	BASETP2	DEEPFR3

173 **Table S3** Sensitivity ranking of HSPF parameters for *E. coli* simulation with respect to Mean
 174 Square Error. Number in parameter represents land-use; 1: Forest, 2: Teak, 3: Fallow, and 4:
 175 Annual crop

Rank	Parameter
1	WSQOP3
2	WSQOP2
3	SQOLIM_MF2
4	WSQOP1
5	SQOLIM_MF3
6	WSQOP4
7	SQOLIM_MF1
8	FSTDEC
9	THFST
10	SQOLIM_MF4
11	AOQC4
12	AOQC2
13	AOQC3
14	AOQC1
15	IOQC3
16	IOQC2
17	IOQC4
18	IOQC1

176

177

178 **References**

179 Boithias, L., Auda, Y., Audry, S., Bricquet, J. p., Chanhphengxay, A., Chaplot, V., de Rouw, A.,
180 Henry des Tureaux, T., Huon, S., and Janeau, J. l.: The Multiscale TROPICAL CatchmentS critical
181 zone observatory M-TROPICS dataset II: land use, hydrology and sediment production

182 monitoring in Houay Pano, northern Lao PDR, *Hydrological Processes*, 35, e14126, 2021a

183

184 Collins, R., and Neal, C.: The hydrochemical impacts of terraced agriculture, Nepal. *Science of*
185 *the total environment*, 212(2-3), 233-243, 1998.

186

187 Hochreiter, S., and Schmidhuber, J.: Long short-term memory. *Neural computation*, 9(8), 1735-
188 1780, 1997.

189

190 Kim, M., Boithias, L., Cho, K. H., Silvera, N., Thammahacksa, C., Latsachack, K., ... and
191 Ribolzi, O.: Hydrological modeling of fecal indicator bacteria in a tropical mountain catchment.
192 *Water research*, 119, 102-113. 2017.

193

194 Moriasi, D. N., Arnold, J. G., Van Liew, M. W., Bingner, R. L., Harmel, R. D., and Veith, T. L.:
195 Model evaluation guidelines for systematic quantification of accuracy in watershed simulations.
196 *Transactions of the ASABE*, 50(3), 885-900, 2007.

197

198 QGIS Development Team.: QGIS geographic information system. *Open source geospatial*
199 *foundation project*, 2016.

200

201 Ribolzi, O., Evrard, O., Huon, S., De Rouw, A., Silvera, N., Latsachack, K. O., ... and
202 Sengtaheuanghong, O.: From shifting cultivation to teak plantation: effect on overland flow and
203 sediment yield in a montane tropical catchment. *Scientific Reports*, 7(1), 1-12. 2017.

204

205 Ribolzi, O., Evrard, O., Huon, S., Rochelle-Newall, E., Henri-des-Tureaux, T., Silvera, N., ... and
206 Sengtaheuanghong, O.: Use of fallout radionuclides (^7Be , ^{210}Pb) to estimate resuspension of
207 *Escherichia coli* from streambed sediments during floods in a tropical montane catchment.
208 *Environmental Science and Pollution Research*, 23(4), 3427-3435, 2016.

209

210 Ribolzi, O., Lacombe, G., Pierret, A., Robain, H., Sounyafong, P., De Rouw, A., ... and
211 Latsachak, K. O.: Interacting land use and soil surface dynamics control groundwater outflow in
212 a montane catchment of the lower Mekong basin. *Agriculture, Ecosystems & Environment*, 268,
213 90-102. <https://doi.org/10.1016/j.agee.2018.09.005>, 2018.

214

215

216 Waseem, M., Mani, N., Andiego, G., and Usman, M.: A review of criteria of fit for hydrological
217 models. *International Research Journal of Engineering and Technology (IRJET)*, 4(11), 1765-
218 1772, 2017.